

## Quantum Limits of Transmission Electron Microscopy

Christian Dwyer<sup>\*</sup>

*Electron Imaging and Spectroscopy Tools, PO Box 506, Sans Souci, NSW 2219, Australia  
and Physics, School of Science, RMIT University, Melbourne, Victoria 3001, Australia*



(Received 8 July 2022; accepted 26 December 2022; published 31 January 2023)

New-generation transmission electron microscopes (TEMs) are equipped with detectors that approach the shot-noise limit. Hence it is pertinent to ask: What are the quantum limits of electron scattering experiments in the TEM? For example, for a given electron dose, what is the ultimate accuracy allowed by quantum mechanics for the atomic structure of a material? We provide quantitative answers based on quantum estimation theory. We also show that, for an arbitrary set of sample parameters, the quantum limit is achievable under conditions of weak scattering, but not strong multiple scattering (this conclusion extends to scattering of other types of radiation). Implications for structure determination of radiation-sensitive materials are discussed.

DOI: 10.1103/PhysRevLett.130.056101

In his famous 1959 lecture, “There’s Plenty of Room at the Bottom,” Richard Feynman put forward a challenge to improve the then-current resolution of the electron microscope “by 100 times” [1]. That challenge was effectively met in subsequent decades by transmission electron microscopy (TEM) and scanning tunneling microscopy (STM). Here we focus on TEM, which is capable of imaging the atomic structure of materials beyond their surface layers. Around the turn of the century, aberration-corrected electron optics [2] pushed the spatial resolution of TEM into the deep-sub-Ångström regime. Moreover, the last decade has seen the realization of a new class of electron detectors having dramatically improved speeds and sensitivities that can approach the shot-noise limit [3]. This has completely opened the door to “low-dose” electron imaging and diffraction of radiation-sensitive materials, such as two-dimensional materials, and soft and biological materials. In fact, in the not-too-distant future, the precision of TEM experiments will likely approach the fundamental limits imposed by quantum mechanics. Hence, it is timely to consider: What *are* the quantum limits of electron beam techniques in the TEM? For example, what is the ultimate accuracy attainable for the position of an atom in a material? What determines this accuracy, and can it be achieved in practice? The answers determine our ability to “know” the atomic structure and other characteristics of materials, most especially radiation-sensitive materials.

Here, we provide answers using quantum estimation theory. In recent years, the range of applications of quantum estimation theory has grown steadily (see Refs. [4] for reviews). Here, we elucidate how the formalism applies to electron scattering experiments in the TEM, with an emphasis on the multiple scattering problem. We derive the quantum limit of precision for materials atomic structure determination in the TEM, which constitutes an

explicit quantitative limit for a given electron dose. We also show that, for a simultaneous estimate of an arbitrary set of sample parameters, the quantum limit can be achieved under weak scattering conditions, but it cannot be achieved when there is strong multiple scattering.

*Quantum estimation in TEM.*—Consider an electron scattering experiment in a TEM, designed to measure, simultaneously, a set of parameters of interest, whereby a suitable electron-optical arrangement is used to pass a fixed coherent beam of electrons through an electron-transparent sample to generate an image, diffraction pattern, or hologram, etc. The parameters, denoted  $\lambda_1, \dots, \lambda_P$ , are assumed real, but they require no Hermitian operator representation. Pertinent examples are parameters characterizing a given sample (our main focus) and/or parameters characterizing the electron optics. The relevant quantum state is that of the scattered electrons impinging on the detector, denoted  $|\psi\rangle$ , which is assumed to depend continuously on  $\lambda_1, \dots, \lambda_P$ , and have normalization  $\langle\psi|\psi\rangle = 1$ . In this first Letter, we restrict ourselves to elastic scattering, consistent with the assumption of a pure state  $|\psi\rangle$ .

It can be shown [5] that the variance of an (unbiased) estimate of the  $\mu$ th parameter  $\lambda_\mu$ , obtained from  $N$  repeated quantum measurements, satisfies, in the limit of large  $N$ , the following chain of inequalities:

$$\text{Var}[\lambda_\mu] \geq I_{\mu\mu}^{-1} \geq J_{\mu\mu}^{-1}. \quad (1)$$

Here  $I$  is the well-known (classical) Fisher information matrix (CFIM), and  $J$  is the quantum Fisher information matrix (QFIM, defined below). Relation (1) involves diagonal elements of the inverse matrices. The first inequality in (1) is the well-known Cramer-Rao inequality dictating the precision of any (unbiased) statistical estimator. The CFIM  $I$  depends on the complete experimental setup,

including the process used to detect  $|\psi\rangle$ . By contrast, the QFIM  $J$  is independent of the detection process or any influence that comes “after” the parameters  $\lambda_1, \dots, \lambda_P$ .  $J$  dictates the ultimate precision compatible with quantum mechanics,  $\text{Var}[\lambda_\mu] = J_{\mu\mu}^{-1}$ , known as the *quantum Cramer-Rao bound* (QCRB). Only an *optimal* simultaneous estimate achieves the QCRB  $\forall \lambda_1, \dots, \lambda_P$ , which requires both  $I = J$  and an estimator that achieves the (classical) Cramer-Rao bound.

For a pure state  $|\psi\rangle$ , the  $\mu\nu$ th element of the QFIM is

$$J_{\mu\nu} \equiv 4N \text{Re} \langle \partial_\mu \psi | \hat{Q} | \partial_\nu \psi \rangle. \quad (2)$$

Here,  $N$  is interpreted as the number of beam electrons used in the TEM experiment, giving rise to the shot-noise (standard quantum) limit of precision.  $|\partial_\mu \psi\rangle$  is the partial derivative of  $|\psi\rangle$  with respect to  $\lambda_\mu$ .  $\hat{Q} \equiv \mathbb{1} - |\psi\rangle\langle\psi|$  projects the component orthogonal to  $|\psi\rangle$ .

*Simultaneous estimation of sample parameters.*—We adopt a common forward-scattering formalism,  $|\psi\rangle = \hat{U}|\psi_0\rangle$ , where  $\hat{U}$  is a unitary operator and  $|\psi_0\rangle$  is some initial state. We write  $\hat{U} = \hat{A}\hat{S}$ , where the unitary  $\hat{S}$  describes the scattering in the sample, and the unitary  $\hat{A}$  describes the effect of the postsample electron optics.

To accommodate the full range of samples studied in TEM,  $\hat{S}$  must be capable of describing multiple scattering. For a sample of thickness  $t$ ,  $\hat{S}$  can be written as a multiplicative integral

$$\hat{S}(t, 0) = [1 - i(\hat{T} + \hat{V}_{N_S})\Delta z] \cdots [1 - i(\hat{T} + \hat{V}_1)\Delta z], \quad (3a)$$

where  $\hat{T}$  is the “transverse kinetic energy” operator and  $\hat{V}_n$  is the potential operator for the  $n$ th plane of the sample. The impulse limit  $N_S \rightarrow \infty$  and  $\Delta z \rightarrow 0$  as  $N_S \Delta z = t$  is implied, in which case the  $\hat{V}_n$ ’s form an operator  $\hat{V}(z)$  depending continuously on depth  $z$ , analogous to a time-dependent potential energy.  $\hat{V}(z)$  is diagonal in the 2D (transverse) position space:

$$\hat{V}(z) = \frac{1}{M} \sum_{\mathbf{x}} |\mathbf{x}\rangle v(\mathbf{x}, z) \langle \mathbf{x}|, \quad (3b)$$

where  $v(\mathbf{x}, z)$  is the 3D electrostatic potential, and  $M$  is the number of points in the 2D discretization [6].  $\hat{T}$  is diagonal in the 2D (transverse) Fourier space:

$$\hat{T} = \sum_{\mathbf{k}} |\mathbf{k}\rangle \zeta(\mathbf{k}) \langle \mathbf{k}|, \quad (3c)$$

where  $\zeta(\mathbf{k}) = \pi \lambda_e |\mathbf{k}|^2$  is the paraxial phase shift per unit  $z$ , which involves the electron wavelength  $\lambda_e$ .

From here onwards, we let  $\lambda_1, \dots, \lambda_P$  be characteristic parameters of the sample as they are the primary aim of most TEM experiments. Such a choice is appropriate when

the other experimental parameters, such as those characterizing the electron optics, are sufficiently well known, e.g., from auxiliary measurements, as is often done in practice. Thus,  $\hat{S}$  depends on  $\lambda_1, \dots, \lambda_P$  [through  $\hat{V}(z)$ ], but  $|\psi_0\rangle$  and  $\hat{A}$  do not. Hence

$$|\partial_\mu \psi\rangle = \hat{A} \hat{S}_\mu(t, 0) |\psi_0\rangle, \quad (4)$$

where  $\hat{S}_\mu \equiv \partial_\mu \hat{S}$ . Using (3a) and (4) in (2), we obtain

$$J_{\mu\nu} = 4N \text{Re} \langle \psi_0 | \hat{W}_\mu \hat{Q}_0 \hat{W}_\nu | \psi_0 \rangle, \quad (5a)$$

$\hat{W}_\mu \equiv \hat{S}^\dagger i \hat{S}_\mu$  is a Hermitian generator, and  $\hat{Q}_0 \equiv \mathbb{1} - |\psi_0\rangle\langle\psi_0|$  [see Supplemental Material (SM) [7] for derivation]. An explicit form for  $\hat{W}_\mu$  is given by

$$\hat{W}_\mu = \int_0^t dz \hat{S}(0, z) \hat{V}_\mu(z) \hat{S}(z, 0), \quad (5b)$$

where  $\hat{V}_\mu \equiv \partial_\mu \hat{V}$ , and the symmetry  $\hat{S}^\dagger(z', z) = \hat{S}(z, z')$  has been used. The operator  $\hat{V}_\mu(z)$  has the form (3b) except that  $v(\mathbf{x}, z)$  is replaced by  $v_\mu(\mathbf{x}, z) \equiv \partial_\mu v(\mathbf{x}, z)$ .

$J$  given by Eqs. (5) determines the *quantum limit of sample parameter estimation in the TEM* (for general multiple scattering conditions). Because here  $J$  refers to sample parameters only, it is *independent of any post-sample electron optics or detector*. Hence this  $J$  applies to any TEM modality, whether it be imaging, diffraction, holography, or some other modality.

Table I lists a hierarchy of scattering approximations common in the fields of TEM and coherent x-ray imaging and diffraction, along with expressions for the corresponding QFIM on sample parameters (see SM for derivations). Table I is roughly in order of decreasing scattering strength (and therefore decreasing generality), and it applies to arbitrary sample parameters so as to accommodate a very broad range of situations. The phase-object approximation (POA) applies to thin samples in which the transverse components of scattering paths are negligible (e.g., 2D materials). The more stringent weak POA (WPOA) is often used to describe scattering in biological samples in TEM. The simplicity of the POA and WPOA enable some important insights presented next. The remainder of Table I will be discussed later.

*Implications for atomic structure determination.*—Here we let the parameters be the lateral (2D) Cartesian coordinates  $x_\mu$  of the atoms in the sample. We adopt the POA (or WPOA) and assume normal plane wave illumination  $|\psi_0\rangle = |\mathbf{k}_0 = \mathbf{0}\rangle$ . Under these conditions, we can obtain, for coordinates  $x_\mu$  and  $x_\nu$ , which may refer to different atoms or the same atom, the QFIM elements

$$J_{\mu\nu} = \frac{4Nt^2}{a} \int d^2\mathbf{x} v_\mu(\mathbf{x}) v_\nu(\mathbf{x}), \quad (6)$$

TABLE I. Hierarchy of Scattering Approximations and Corresponding Quantum Fisher Information on Sample Parameters.

Name	$\hat{S}(t, 0)$	$J_{\mu\nu}$	$\langle \psi_0   [\hat{W}_\mu, \hat{W}_\nu]   \psi_0 \rangle = 0?^a$
General multiple scattering	Eqs. (3)	Eqs. (5)	No
Projection approximation (PA)	$\exp[-it(\hat{T} + \hat{V})]$	Eqs. (5), $\hat{V}$ independent of $z$	No
Phase-object approximation (POA)	$\exp[-it\hat{V}], (\hat{T} = 0)$	$4Nt^2[\langle \hat{V}_\mu \hat{V}_\nu \rangle - \langle \hat{V}_\mu \rangle \langle \hat{V}_\nu \rangle]$	Yes
Pseudo-weak POA (PWPOA)	$e^{-it\hat{T}} - i \int_0^t dz e^{-i(t-z)\hat{T}} \hat{V} e^{-iz\hat{T}}$	$4Nt^2[\langle \hat{V}_\mu \text{sinc}^2(t\hat{T}/2) \hat{V}_\nu \rangle - \langle \hat{V}_\mu \rangle \langle \hat{V}_\nu \rangle]$	Yes <sup>b</sup>
Weak POA (WPOA)	$1 - it\hat{V}, (\hat{T} = 0)$	$4Nt^2[\langle \hat{V}_\mu \hat{V}_\nu \rangle - \langle \hat{V}_\mu \rangle \langle \hat{V}_\nu \rangle]$	Yes

<sup>a</sup>Applies to the case of arbitrary sample parameters  $\lambda_1, \dots, \lambda_p$  and an initial state  $|\psi_0\rangle$  not dependent on them.

<sup>b</sup>Holds when the initial state  $|\psi_0\rangle$  free-propagates along  $z$  with uniform phase shift.

where  $N/a$  is the ‘‘electron dose’’ ( $a$  is the area of the transverse plane) (see SM for derivation).  $J^{-1}$  obtained from (6) provides the *QCRB of atomic structure determination in the TEM* (for the stated conditions). Commonly,  $v(\mathbf{x})$  is approximated by a sum of atomic potentials, and  $v_\mu(\mathbf{x})$  has the form of a dipole at the atom’s location directed along  $x_\mu$ .

Before proceeding, we recall that the QCRB is valid asymptotically, that is, for  $N$  large enough for the statistics to become Gaussian. To obtain results outside the asymptotic regime, we make use of the quantum Ziv-Zakai bound (QZZB) [8]. The QZZB applies to arbitrary  $N$ , and in the asymptotic regime it essentially coincides with the QCRB (their ratio being QZZB/QCRB  $\approx$  0.61). We use the QZZB to gauge the onset of the asymptotic regime where the QCRB applies (see SM for further details). (Though valid for any  $N$ , the QZZB has drawbacks in that there is no guarantee of attaining it [8], and it does not so readily suggest routes to optimized experimental design, hence our focus on the QCRB.)

As a simple, yet highly illustrative, example, Fig. 1 shows the quantum limit of precision (square root of variance) in the lateral coordinate of single isolated atoms as a function of electron dose. The plot shows the greater of the QZZB and the QCRB (which in practice means the QZZB at lower doses and the QCRB at higher doses). Results are presented for a selection of atomic species and for beam energies in the range 30–300 keV (representative of modern TEMs). In Fig. 1, we observe a very strong ‘‘threshold effect’’ where, for a given species and beam energy, increasing the dose above a certain threshold sees the statistics ‘‘suddenly’’ enter the asymptotic regime. In this regime, the attainable precision is better than  $0.1 \text{ \AA}$  for all elements and beam energies, improving as  $1/\sqrt{N/a}$ . Interestingly, for all elements, the precision at threshold falls in a narrow range around  $0.05 \text{ \AA}$ . For doses below threshold, the QZZB indicates a rapid deterioration in the achievable precision, with atomic-level precision quickly becoming completely lost. For gold (strong scatterer) the threshold is 15–100  $e^-/\text{\AA}^2$ , whereas for carbon (weak scatterer) it is 500–2000  $e^-/\text{\AA}^2$ . Lower beam energies can achieve better precision owing to the stronger interaction (other factors being equal).

As carbon is representative of biological materials, and such materials can often tolerate doses of only  $\lesssim 10 e^-/\text{\AA}^2$  before noticeable damage [9], Fig. 1 confirms that achieving sub- $\text{\AA}$  precision from a single TEM exposure is an utterly hopeless task. However, if the sample can be cloned in vast numbers, then the dose can be distributed and the damage limit can be overcome. Cryo-TEM imaging of proteins is an excellent example of this strategy (though in this case each protein’s orientation must still be determined). Other radiation-sensitive materials, such as covalent organic frameworks, have comparable dose tolerances [10], and similar remarks apply.

A diagonal element  $J_{\mu\mu}$  in (6) typically directly influences the QCRB for the atomic coordinate  $x_\mu$  (as in Fig. 1). However, the *off*-diagonals referring to two different atoms can also play an important role if those atoms overlap significantly when viewed along the beam direction. Such off-diagonals lead to covariances which worsen

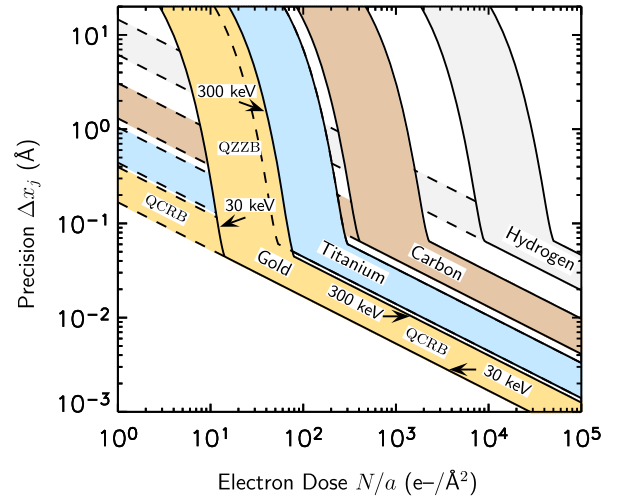


FIG. 1. Quantum limit of precision in the lateral coordinate of single atoms, as a function of precision in the lateral coordinate of single atoms, as a function of electron dose and beam energy. Each solid line shows the QZZB at lower doses (nonasymptotic regime) and the QCRB at higher doses (asymptotic regime). For each atomic species, lower and upper solid lines bordering the colored band correspond to 30 and 300 keV electron beams. In the background, dashed straight lines show the QCRB in the nonasymptotic regime.

the attainable precision of coordinate estimates. In cases where atoms of the same species overlap completely to form an “atomic column,” as often encountered when crystalline materials are aligned at major zone axes, the QFIM becomes singular, indicating a complete loss of precision for the atomic coordinates involved. In such cases, reparametrization of the QFIM is necessary, e.g., using column coordinates rather than atom coordinates. We note that, for a homogenous column that is well separated from any others, Fig. 1 readily applies after a simple scaling by the number of atoms in the column (though keeping in mind the limitations of the employed POA).

Further general remarks are possible if we consider the *rotational average* of the QFIM in (6), that is, the QFIM relevant to a sample whose 3D orientation in the TEM is “random.” This situation is especially relevant to cryo-TEM imaging of proteins and other biological structures. We find that, for structures without too much symmetry, the off-diagonal terms worsen the achievable precision typically by only a few percent, that is, their effect is often negligible, so that the QCRB for a 3D Cartesian coordinate of an atom is essentially what it would be if the atom were isolated (apart from a factor  $\sqrt{3/2}$  coming from the 3D rotational average) (further details in SM). Put simply, the rotational average can be extremely effective in removing the off-diagonals in (6).

*Conditions for optimal estimation.*—We assume that the detection of  $|\psi\rangle$  is described by a projection-valued measure (PVM), where a possible outcome  $\xi$  occurs with probability  $p(\xi) = |\langle\xi|\psi\rangle|^2$ . It can be shown [11] (and see SM) that  $I = J$ , thus achieving the second equality in (1), if and only if

$$\langle\psi_0|[\hat{W}_\mu, \hat{W}_\nu]|\psi_0\rangle = 0 \quad \forall \mu \text{ and } \nu, \quad (7a)$$

$$\text{Im}\{\langle\psi|\xi\rangle\langle\xi|\hat{Q}|\partial_\mu\psi\rangle\} = 0 \quad \forall \xi \text{ and } \mu. \quad (7b)$$

As discussed in [11], if (7a) is satisfied, then it is possible to satisfy (7b) by constructing a PVM from the  $P + 1$  states  $\{|\psi\rangle, \hat{Q}|\partial_1\psi\rangle, \dots, \hat{Q}|\partial_P\psi\rangle\}$ . Implementing such a PVM experimentally is challenging, and in general it requires prior knowledge of the said states.

However, TEM phase-contrast imaging is a case where the conditions (7) can be more readily realized. For TEM imaging, the experimental setup includes the objective lens postfield aberrations and a pixelated detector. The new-generation pixelated electron detectors referred to in the introduction constitute a reasonable approximation to a PVM, where each measurement results in a scattered electron registered by some pixel at position  $\mathbf{x}$  with probability  $p(\mathbf{x}) = |\langle\mathbf{x}|\psi\rangle|^2$ . If we adopt the WPOA (Table I), then (7a) is satisfied (see SM), and for an incident plane wave  $|\psi_0\rangle = |\mathbf{k}_0\rangle$ , (7b) reduces to

$$\text{Re}\langle\mathbf{k}_0|\hat{A}^\dagger|\mathbf{x}\rangle\langle\mathbf{x}|\hat{A}[\hat{V}_\mu - \langle\hat{V}_\mu\rangle]|\mathbf{k}_0\rangle = 0, \quad (8)$$

which is satisfied for aberration phase shifts  $\gamma(\mathbf{k} + \mathbf{k}_0) - \gamma(\mathbf{k}_0) = (1 - \delta_{\mathbf{k}\mathbf{0}})[\pi/2 + \phi(\mathbf{k})] \pmod{2\pi}$ , where  $\phi(\mathbf{k})$  is any odd function of  $\mathbf{k}$  (see SM). This is the famous Zernike phase condition (ZPC) [12] (in generalized form). The ZPC is remarkable in that no prior knowledge of the sample is required. So far, no mention has been made of the actual statistical estimator to be used. However, as is well known, a model-based maximum-likelihood estimator (MLE) constitutes an efficient and unbiased estimation in that it achieves, asymptotically, the Cramer-Rao bound, that is, the first equality in (1). Hence, within the stated approximations and idealizations, the ZPC combined with MLE achieves the quantum limit in the simultaneous estimate of an arbitrary set of sample parameters (for parameters that are consistent with the WPOA).

For strong multiple scattering conditions, we can show that *condition (7a) does not hold* (see Table I and SM), that is, no optimal simultaneous estimate is possible, that is, while we can calculate the QCRB using (5), *no measurement scheme can actually achieve it*. Nor does (7a) hold for the projection approximation (PA) where  $\hat{V}$  is independent of  $z$ . On the other hand, (7a) does hold for the POA obtained by setting  $\hat{T} = 0$ . The WPOA is a special case of the POA, and so (7a) holds in that case too, consistent with the previous paragraph. The pseudo-weak POA (PWPOA) is a single-scattering approximation in which  $\hat{T} \neq 0$ , and (7a) holds for initial states that free-propagate along  $z$  with uniform phase shift (see SM for further details).

*Discussion.*—The importance of the ZPC in the TEM is well-established [12], and achieving it is nontrivial, with several methods having been pursued, including balancing of lens aberrations [13], and electrostatic- [14], matter- [15], and photon-based [16] phase plates. However, it is likely not widely appreciated that the ZPC coupled with MLE can achieve *the quantum limit* of precision for *an arbitrary set* of sample parameters under weak-scattering conditions. While the weak-scattering regime is necessarily limited, it does encompass several important classes of materials, including many two-dimensional materials, and soft and biological materials. Such materials are very often radiation sensitive, and so the benefits of an optimized measurement scheme are manifest. Under the less stringent POA, no analogue of the ZPC, whereby optimality is achieved via sample-independent phase shifts, exists. But an optimal scheme for the POA *is* possible, and has been reported for optical microscopy [17], although it requires *a priori* knowledge of the coordinate space phase shifts for the specific sample. In general, (7) can be viewed as a guiding condition for optimized experimental design.

For general multiple scattering conditions, it is the lateral motion of beam electrons in the sample, as described by the operator  $\hat{T}$ , which is ultimately responsible for the impossibility of achieving the aforementioned quantum limit. When the parameters are atomic coordinates, condition (7a) tends to be violated for atoms that are not well-separated

laterally, such that the scattering from one atom influences the scattering from the other. The news is not all bad, however, since the achievable precision is likely to approach the quantum limit within a factor of order unity [11]. Alternatively, if we are willing to sacrifice the precision of certain sample parameters for the sake of others, or assume that certain ones are known and can be omitted, such that (7a) is satisfied, then it again becomes possible to achieve the quantum limit in the strong multiple scattering regime. An extreme example is single parameter estimation, where (7a) holds trivially and an optimal PVM always exists (e.g.,  $\{|\psi\rangle, \hat{Q}|\partial_\lambda\psi\rangle\}$ ). We also remind the reader that Table I intentionally makes no assumptions regarding the sample parameters, and hence an optimal simultaneous estimation may be possible in special cases.

In the present Letter, we have necessarily made several idealizations in order to demonstrate the quantum limits. For example, the assumption of a PVM comprising a complete set of states amounts to a detector with an ideal point-spread function (PSF) which can fully track the changes in scattering which would result from a variation of the parameter values. These assumptions are approximately fulfilled by new-generation pixelated electron detectors, and continued advances should see them fulfilled even more accurately in the coming decade. Notwithstanding this, the assumption of an ideal PSF can be dropped by employing the more general notion of a positive-operator valued measure. Similarly, there are other factors not explicitly considered here, such as the partial temporal and spatial coherence of the electron beam, electron-optical instabilities, and sample structural disorder, all of which can be incorporated by employing a mixed, as opposed to pure, state description of the scattering. An in-depth analysis will form a forthcoming publication.

We conclude by mentioning several other avenues of quantum estimation in the TEM worthy of further study, namely, sample parameters other than atomic coordinates, electron-optical parameters, incorporation of *a priori* constraints to aid dose reduction [18], quantitative imaging in scanning TEM (STEM) [19], optimized illumination for estimation of a single parameter [20], and consideration of inelastic electron scattering and electron energy-loss spectroscopy (EELS). It is hoped that the present Letter will stimulate further analysis of these (and other) avenues, to aid the design and optimization of existing and new techniques based on electron scattering, and to push the precision of electron beam analysis of materials ever closer to the quantum limits [7].

---

\*dwyer@eistools.com

[1] R. P. Feynman, *Caltech Eng. Sci.* **23**, 22 (1960).  
 [2] M. Haider, S. Uhlemann, E. Schwan, H. Rose, B. Kabius, and K. Urban, *Nature (London)* **392**, 768 (1998); P. Batson,

- N. Dellby, and O. L. Krivanek, *Nature (London)* **418**, 617 (2002).  
 [3] B. Bammes, R. Rochat, J. Jakana, D. Chen, and W. Chiu, *J. Struct. Biol.* **177**, 589 (2012); G. McMullan, A. Faruqi, D. Clare, and R. Henderson, *Ultramicroscopy* **147**, 156 (2014); S. Chang, C. Dwyer, J. Bartel, C. Boothroyd, and R. Dunin-Borkowski, *Ultramicroscopy* **161**, 90 (2016); H. Ryll, M. Simson, R. Hartmann, P. Holl, M. Huth, S. Ihle, Y. Kondo, P. Kotula, A. Liebel, K. Müller-Caspary, A. Rosenauer, R. Sagawa, J. Schmidt, H. Soltau, and L. Strüder, *J. Instrum.* **11**, P04006 (2016); Y. Jiang, Z. Chen, Y. Han, P. Deb, H. Gao, S. Xie, P. Purohit, M. W. Tate, J. Park, S. M. Gruner, V. Elser, and D. A. Muller, *Nature (London)* **559**, 343 (2018); I. MacLaren, T. A. Macgregor, C. S. Allen, and A. I. Kirkland, *APL Mater.* **8**, 110901 (2020); C. Dwyer, *J. Phys. Mater.* **4**, 042006 (2021).  
 [4] J. Liu, H. Yuan, X. M. Lu, and X. Wang, *J. Phys. A* **53**, 023001 (2020); J. S. Sidhu and P. Kok, *AVS Quantum Sci.* **2**, 014701 (2020).  
 [5] S. L. Braunstein and C. M. Caves, *Phys. Rev. Lett.* **72**, 3439 (1994); S. L. Braunstein, C. M. Caves, and G. J. Milburn, *Ann. Phys. (N.Y.)* **247**, 135 (1996).  
 [6] Conventions used:  $\hat{\mathbb{I}} = \sum_k |k\rangle\langle k| = (1/M) \sum_x |x\rangle\langle x|$ ,  $\langle x|x'\rangle = M\delta_{xx'}$ ,  $\langle k|k'\rangle = \delta_{kk'}$ , and  $\langle x|k\rangle = e^{2\pi i k \cdot x} v(x, z)$  is the 3D electrostatic potential times  $(\hbar v)^{-1}$ ,  $v$  is the beam electron speed.  $|\psi\rangle$  omits a trivial factor  $e^{2\pi i z/\lambda_e}$ .  
 [7] See Supplemental Material at <http://link.aps.org/supplemental/10.1103/PhysRevLett.130.056101> for derivations and auxiliary details.  
 [8] J. Ziv and M. Zakai, *IEEE Trans. Inf. Theory* **15**, 386 (1969); K. L. Bell, Y. Steinberg, Y. Ephraim, and H. L. Van Trees, *IEEE Trans. Inf. Theory* **43**, 624 (1997); M. Tsang, *Phys. Rev. Lett.* **108**, 230401 (2012); D. W. Berry, M. Tsang, M. J. W. Hall, and H. M. Wiseman, *Phys. Rev. X* **5**, 031018 (2015); J. Rubio, P. Knott, and J. Dunningham, *J. Phys. Commun.* **2**, 015027 (2018).  
 [9] J. Frank, *Three-Dimensional Electron Microscopy of Macromolecular Assemblies*, 2nd ed. (Oxford University Press, USA, 2006).  
 [10] Q. Chen, C. Dwyer, G. Sheng, C. Zhu, C. Zheng, and Y. Zhu, *Adv. Mater.* **32**, 1907619 (2020).  
 [11] K. Matsumoto, *J. Phys. A* **35**, 3111 (2002); T. Baumgratz and A. Datta, *Phys. Rev. Lett.* **116**, 030801 (2015); L. Pezze, M. A. Ciampini, N. Spagnolo, P. C. Humphreys, A. Datta, I. A. Walmsley, M. Barbieri, F. Sciarrino, and A. Smerzi, *Phys. Rev. Lett.* **119**, 130504 (2017); F. Belliardo and V. Giovannetti, *New J. Phys.* **23**, 063055 (2021).  
 [12] F. Zernike, *Physica (Amsterdam)* **9**, 686 (1942); H. Boersch, *Z. Naturforsch. Teil A* **2**, 615 (1947); H. Rose, *Ultramicroscopy* **110**, 488 (2010); R. M. Glaeser, *Rev. Sci. Instrum.* **84**, 111101 (2013).  
 [13] O. Scherzer, *J. Appl. Phys.* **20**, 20 (1949); L. Y. Chang, A. I. Kirkland, and J. M. Titchmarsh, *Ultramicroscopy* **106**, 301 (2006); M. Lentzen, *Microsc. Microanal.* **14**, 16 (2008).  
 [14] E. Majorovits, B. Barton, K. Schultheiss, F. Pérez-Willard, D. Gerthsen, and R. R. Schröder, *Ultramicroscopy* **107**, 213 (2007); D. Alloyeau, W. K. Hsieh, E. H. Anderson,

- L. Hilken, G. Benner, X. Meng, F.R. Chen, and C. Kisielowski, *Ultramicroscopy* **110**, 563 (2010).
- [15] K. Nagayama and R. Danev, *Phil. Trans. R. Soc. B* **363**, 2153 (2008); R. Danev, B. Buijsse, M. Khoshouei, J. M. Pnitzko, and W. Baumeister, *Proc. Natl. Acad. Sci. U.S.A.* **111**, 15635 (2014).
- [16] H. Müller, J. Jin, R. Danev, J. Spence, H. Padmore, and R. M. Glaeser, *New J. Phys.* **12**, 073011 (2010); O. Schwartz, J. J. Axelrod, S. L. Campbell, C. Turnbaugh, R. M. Glaeser, and H. Müller, *Nat. Methods* **16**, 1016 (2019).
- [17] T. Juffmann, A. de los Ríos Sommer, and A. Gigan, *Opt. Commun.* **454**, 124484 (2020).
- [18] S. H. W. Scheres, *J. Mol. Biol.* **415**, 406 (2012); T. Sanders and C. Dwyer, *IEEE Trans. Image Process.* **29**, 351 (2020).
- [19] J. M. LeBeau, S. D. Findlay, L. J. Allen, and S. Stemmer, *Phys. Rev. Lett.* **100**, 206101 (2008); C. Dwyer, C. Maunders, C. Zheng, M. Weyland, P. Tiemeijer, and J. Etheridge, *Appl. Phys. Lett.* **100**, 191915 (2012).
- [20] D. Bouchet, S. Rotter, and A. P. Mosk, *Nat. Phys.* **17**, 564 (2021).